Letter

# Pinch-points to half-moons and up in the stars: The kagome skymap

Dominik Kiese,[1,*] Francesco Ferrari,[2,3,*] Nikita Astrakhantsev,[4,*] Nils Niggemann,[5,6,3,*] Pratyay Ghosh,[3,7,*] Tobias Müller,[7] Ronny Thomale,[3,7] Titus Neupert,[4] Johannes Reuther,[5,6,3] Michel J. P. Gingras,[8] Simon Trebst,[1] and Yasir Iqbal[3,†]

[1]*Institute for Theoretical Physics, University of Cologne, 50937 Cologne, Germany*
[2]*Institut für Theoretische Physik, Goethe-Universität Frankfurt, Max-von-Laue-Straße 1, D-60438 Frankfurt am Main, Germany*
[3]*Department of Physics and Quantum Center for Diamond and Emergent Materials (QuCenDiEM), Indian Institute of Technology Madras, Chennai 600036, India*
[4]*Department of Physics, University of Zürich, Winterthurerstrasse 190, 8057 Zürich, Switzerland*
[5]*Dahlem Center for Complex Quantum Systems and Fachbereich Physik, Freie Universität Berlin, D-14195 Berlin, Germany*
[6]*Helmholtz-Zentrum Berlin für Materialien und Energie, D-14109 Berlin, Germany*
[7]*Institute for Theoretical Physics and Astrophysics, Julius-Maximilian's University of Würzburg, Am Hubland, D-97074 Würzburg, Germany*
[8]*Department of Physics and Astronomy, University of Waterloo, Waterloo, Ontario, Canada N2L 3G1*

(Received 30 July 2022; accepted 7 February 2023; published 24 February 2023)

Pinch point singularities, associated with flat band magnetic excitations, are tell-tale signatures of Coulomb spin liquids. While their properties in the presence of quantum fluctuations have been widely studied, the fate of the complementary nonanalytic features—shaped as half moons and stars—arising from adjacent shallow dispersive bands has remained unexplored. Here, we address this question for the spin $S = 1/2$ Heisenberg antiferromagnet on the kagome lattice with second and third neighbor couplings, which allows one to tune the classical ground state characterized by flat bands to one that is governed by shallow dispersive bands for intermediate coupling strengths. Employing the complementary strengths of variational Monte Carlo, pseudofermion functional renormalization group, and density-matrix renormalization group, we establish the quantum phase diagram of the model. The $U(1)$ Dirac spin liquid ground state of the nearest-neighbor antiferromagnet remains remarkably robust till intermediate coupling strengths when it transitions into a pinwheel valence bond crystal displaying signatures of half moons in its structure factor. Our Letter thus identifies a microscopic setting that realizes one of the proximate orders of the Dirac spin liquid identified in a recent work [Song, Wang, Vishwanath, and He, Nat. Commun. **10**, 4254 (2019)]. For larger couplings, we obtain a collinear magnetically ordered ground state characterized by starlike patterns.

DOI: 10.1103/PhysRevResearch.5.L012025

Classical spin models which admit a completion of squares belong to the distinct *genre* of "maximally frustrated" Hamiltonians which feature an exponentially large degenerate ground-state manifold [1,2]. In two spatial dimensions, a celebrated example is the classical nearest-neighbor Heisenberg antiferromagnet (NNHAF) on the kagome lattice:

$$\mathcal{H} = J_1 \sum_{\langle ij \rangle} \mathbf{S}_i \cdot \mathbf{S}_j = \frac{J_1}{2} \sum_{\Delta,\nabla} (\mathbf{S}_1 + \mathbf{S}_2 + \mathbf{S}_3)^2 - J_1 N, \quad (1)$$

with $|\mathbf{S}_i| = 1$ and $N$ the total number of spins. By virtue of the right-hand side of Eq. (1), any spin configuration which satisfies $(\mathbf{S}_1 + \mathbf{S}_2 + \mathbf{S}_3) = 0$ on each triangle qualifies as a classical ground state.

This local constraint leads to the formation of a Coulomb spin liquid [3], with algebraically decaying spin-spin correlations in real space giving some structure to the exponentially large manifold of degenerate classical ground states. In Fourier space, these correlations most strikingly manifest themselves in the presence of nonanalytic features in the structure factor called *pinch points* [4,5]. Remarkably, this classical Coulomb phase remains stable [6,7] even in the presence of additional couplings along a fine-tuned line when second neighbor ($J_2$) and third neighbor along the bonds ($J_{3a}$) [see Fig. 1(a)] of equal strength are concurrent, i.e., $J_2 = J_{3a}$ ($\equiv J$ henceforth). This can be readily understood when diagonalizing the spin exchange Hamiltonian in momentum space, $\mathcal{H}(\mathbf{k})$ [8–10], which reveals that the characteristic flat band of the NNHAF persists [6] up to $J/J_1 = 1/5$. For $J/J_1 > 1/5$, a shallow dispersive band starts to cut below the flat band in parts of the Brillouin zone, which in turn gives rise to pairs of *half moons* [11,12], i.e., crescent shaped arcs in the static structure factor [6], with the flat band remaining close by with a multitude of low-energy excitations [13]. At a deeper level, the formation of half moons in the static structure factor results from a nonanalyticity in the dispersive-band eigenvectors as a function of wave vector which, given the

*These authors contributed equally to this work.
†yiqbal@physics.iitm.ac.in

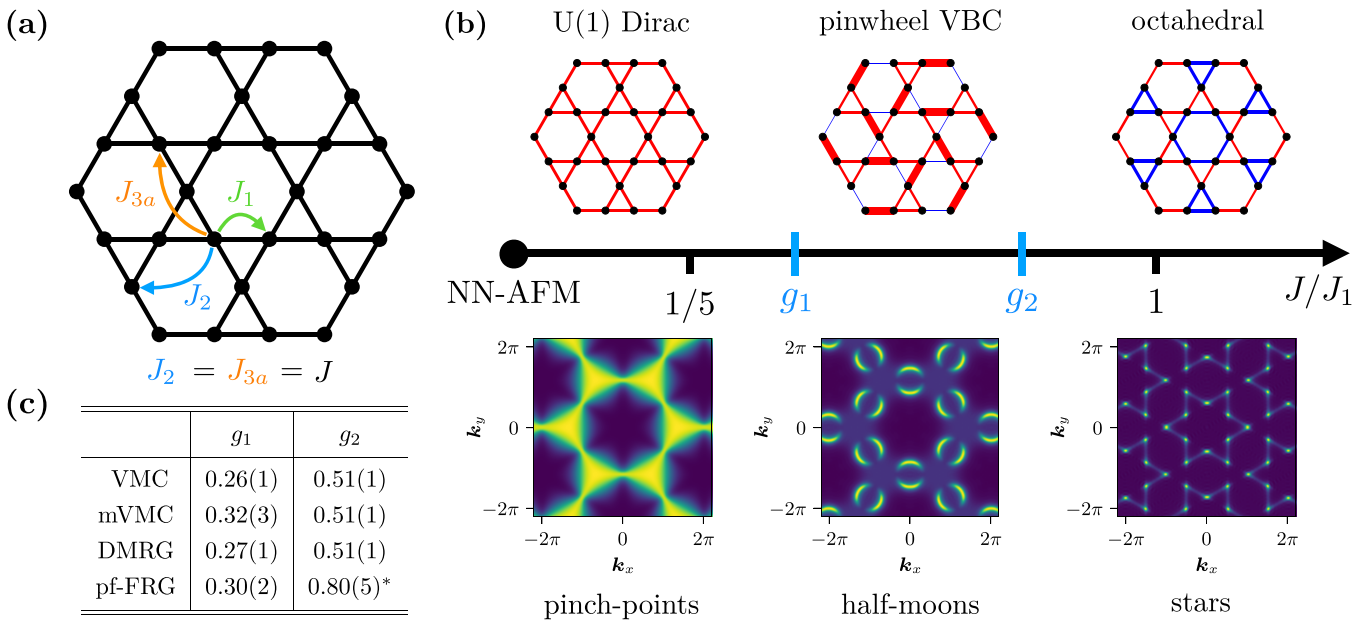


(c)

| | $g_1$ | $g_2$ |
|---|---|---|
| VMC | 0.26(1) | 0.51(1) |
| mVMC | 0.32(3) | 0.51(1) |
| DMRG | 0.27(1) | 0.51(1) |
| pf-FRG | 0.30(2) | 0.80(5)* |

FIG. 1. The kagome skymap. (a) Illustration of first ($J_1$), second ($J_2$), and third neighbor interactions along edges ($J_{3a}$) of the kagome lattice for the model (1). (b) The $S = 1/2$ quantum phase diagram with (top panel) representative real space spin-spin correlation profiles, with red (blue) bonds denoting antiferromagnetic (ferromagnetic) correlations, and (lower panel) spin structure factors of the different phases evaluated at $J/J_1 = 0.1$ (DSL), $J/J_1 = 0.4$ (pinwheel VBC), and $J/J_1 = 0.9$ (collinear order) from pf-FRG. (c) Estimates of the phase boundaries ($g_1$ and $g_2$) obtained from the various approaches employed in this Letter. While we see good agreement within error bars for $g_1$ for all approaches, the pf-FRG result for $g_2$ (marked by an asterisk) shows a notable deviation whose origin is discussed in the Supplemental Material [59].

required completeness of the eigenvector basis, can be viewed as necessarily arising in order to complement the singularity in the wave vector dependence of the flat band eigenvectors [6,14]. With increasing $J/J_1$, the radius of the half moon continuously grows and, at $J/J_1 = 1$, the half moons from different Brillouin zones coalesce, giving rise to a *star* pattern in the static structure factor [6]. While in the case of Ising spins, which show a similar sequence of reciprocal space signatures as a function of $J/J_1$, the nature of the half moons and star phases has a well-understood real space picture in terms of magnetic clustering of topological charges [15–17], for continuous (Heisenberg) spins, the nature of the real space clustering and its freedom to continuously evolve with $J/J_1$ is far more involved and not yet completely understood [6].

Much of the interest in the *quantum* kagome antiferromagnet as a potential host to highly entangled quantum states owes its origin to the realization that its classical ground state is governed by flat bands—an opportunity for otherwise residual quantum effects to dictate the macroscopic ground state. Thence, tuning the pairwise exchange along the maximally frustrated axis ($J_2 = J_{3a} \equiv J$) which, classically, is tuned to have a flat band over an extended region in parameter space, should provide a fertile playground to potentially realize novel states of matter also in the quantum model. For one, the $U(1)$ Dirac spin liquid (DSL) [18–20] ground state of the NNHAF [21–24] is indeed known to be fragile to magnetic order when perturbed by longer-range Heisenberg couplings [25,26] or Dzyaloshinskii-Moriya interactions [27,28], as expected for algebraic spin liquids, but its fate along the maximally frustrated direction of interest here is unknown. In particular, this parameter axis may afford a higher degree of stability to the $U(1)$ DSL against long-range order, and one may wonder whether the DSL naturally gives way to other exotic quantum phases as one marches along this direction. At a conceptual level, instabilities of the DSL have recently been rigorously classified in a field theoretical work [20]. However, it remains an open challenge to identify realistic microscopic settings in which these instabilities manifest themselves and what telltale signatures they display and which might be accessible in experimental studies.

In this Letter, we take an important step in this direction by establishing the quantum counterpart to the classical half-moon phase as a pinwheel valence bond crystal state which the DSL transitions into only for a nonzero critical $J/J_1$ coupling strength. We do so by employing a variety of complementary numerical quantum many-body approaches to build a detailed picture of the $S = 1/2$ quantum phase diagram along the maximally frustrated axis for $J/J_1 > 0$, resolving the characteristic real space and Fourier space signatures of all quantum phases. The numerical approaches include fermionic variational Monte Carlo (VMC) with versatile Gutzwiller projected Jastrow wave functions [29], many-variable variational Monte Carlo (mVMC) with unconstrained optimization of the Bardeen-Cooper-Schrieffer (BCS) pairing function (supplemented with symmetry projectors) [30–38], one-loop pseudofermion functional renormalization group (pf-FRG) [39–48], and density-matrix renormalization group (DMRG) [49,50]. The resulting quantum phase diagram is shown in Fig. 1, where cumulative and complementary evidence from *all* employed approaches shows that the ground state remains nonmagnetic over an appreciably wide span of parameter space [see Fig. 1(b)], notably extending far beyond the

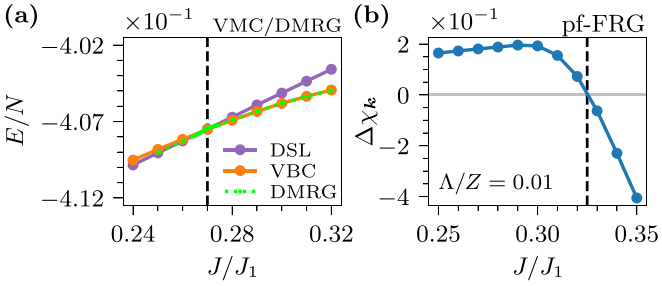


FIG. 2. Transition into half-moon phase. (a) From VMC, the evolution with $J/J_1$ of the energy per site of the DSL and VBC states ($3 \times 12 \times 12$ lattice). DMRG energies are also shown for comparison. (b) From pf-FRG, the variation of the spectral measure $\Delta\chi_{\boldsymbol{k}}$ (see text below) with $J/J_1$ evaluated at the lowest simulated RG cutoff $\Lambda/Z = 0.01$ where $Z = \sqrt{J_1^2 + 2J^2}$.

classical domain ($0 \leqslant J/J_1 \leqslant 0.2$) where flat bands are lowest in energy. This nonmagnetic region is composed of two phases: (i) the $U(1)$ DSL for $0 \leqslant J/J_1 \lesssim g_1$, where $g_1 \approx 0.26$–$0.32$ (see the table in Fig. 1), as characterized by soft maxima at the pinch points in its spin structure factor $\chi(\mathbf{k})$ [51], and (ii) a 12-site unit cell, $C_6$ symmetric pinwheel valence bond crystal (VBC) for $g_1 \lesssim J/J_1 \lesssim g_2$ ($g_2 \approx 0.51$), displaying signatures of half moons in $\chi(\mathbf{k})$ [see Fig. 1(b)]. Our analysis indicates the DSL-VBC transition to be first order as ascertained on finite systems from a sudden change in the spin-spin correlation profile and a crossing of the energies. For $J/J_1 \gtrsim g_2$, the VBC gives way, via a first-order transition, to collinear long-range magnetic order [52,53] with signatures of a starlike pattern in $\chi(\mathbf{k})$. The resemblance of the structure factors of the three quantum phases to the ones of the classical model represents an instance of classical-quantum correspondence previously explored in Refs. [54–57]. A Schwinger boson treatment of this model agrees reasonably well on the location of the phase boundaries but comes to different conclusions regarding the nature of the quantum phases [58].

## I. RESULTS

We set the stage by observing that across our four numerical approaches, we find that the ground-state energy *increases* with $J/J_1$. This behavior is a reflection of an enhanced degree of frustration in this extended kagome antiferromagnet model, which is at variance with the conventional expectation that the NNHAF represents the point of maximal frustration that is relieved upon inclusion of long-range couplings. The occurrence of a pronounced kink in the evolution of the ground-state energy indicates a phase transition [see Fig. 2(a)], and which we estimate to be at $g_1 = 0.27(1)$ via an analysis of its derivative (from our DMRG calculations). This value is also corroborated by the behavior of the von Neumann entanglement entropy which starts decreasing sharply at $g_1$ (Fig. S13 in Supplemental Material [59]) indicating the formation of a less entangled state. To probe the nature of the ensuing states, we start by discussing the results from our fermionic VMC approach with versatile Gutzwiller-projected wave functions, which are constructed such as to allow for an accurate investigation of the competition between nonmagnetic quantum spin liquid (QSL) and VBC phases, together with magnetically ordered states. Such a unified framework has been successfully used for a wide range of frustrated spin models [25,26,60–62]. Our calculations are performed on $3 \times L \times L$ clusters respecting the full symmetry of the kagome lattice. For the $S = 1/2$ NNHAF, there is growing consensus that its ground state is a $U(1)$ DSL [20,21,24,63–66] as it yields the lowest variational energy [21,63]; nonetheless, some recent studies have proposed alternative scenarios of chiral [27,67], gapped $\mathbb{Z}_2$ [68–70], and gapless $\mathbb{Z}_2$ [71] quantum spin liquids. Upon including concurrent $J_2 = J_{3a}$ couplings of identical strength $J$, we assess the potential instability of the $U(1)$ DSL against symmetric $\mathbb{Z}_2$ [72], chiral $U(1)$ [73], chiral $\mathbb{Z}_2$ [74], and lattice nematic $\mathbb{Z}_2$ [75] QSLs. We also probe for possible dimerization tendencies into VBCs with various unit cell sizes up to 36 sites and different symmetries [18,19,76–78]. Our analysis finds a remarkable robustness of the $U(1)$ DSL to the above-mentioned potential instabilities over a wide range along the maximally frustrated axis extending up till $g_1 = 0.26(1)$, which we note is beyond the range $J/J_1 = 1/5$ for the classical model where the flat band excitation is the lowest in energy [6].

At $J/J_1 = 0.26(1)$, we detect a *dimer instability* of the DSL towards a VBC ground state in our VMC calculations. This VBC state is found to be characterized by a $2 \times 2$ enlarged unit cell with a $C_6$ invariant *pinwheel* structure of spin-spin correlations in real space which breaks reflection symmetries [see Fig. 1(b)] [59]. The formation of such a VBC state is further corroborated by an enhanced dimer response (see Fig. S4 in Supplemental Material [59]). Interestingly, such a pattern of strong/weak bonds has previously been identified as descending from confinement transitions of $\mathbb{Z}_2$ spin liquids [79] (left panel of Fig. 1 therein), and recently proposed in Ref. [20] [Fig. 3(c) therein] as a potential instability of the $U(1)$ DSL resulting from a condensation of a $C_6$ invariant mass and the associated monopole terms. Our finding of a $C_6$ symmetric VBC, as opposed to other less symmetric patterns [Fig. 2(c) in Ref. [70]], is likely connected to the fact that an expectation value of the monopole operator which is *imaginary* leads to reflection ($R_y$) symmetry breaking pattern which extremizes the Landau potential [80]. It is worth pointing out that our VBC pattern is distinct from the $2 \times 2$ enlarged VBC patterns previously proposed in Fig. 4 of Ref. [18] and Fig. 5 of Ref. [19] which do not break reflections. Although a monopole which condenses to a *real* expectation value leading to a reflection symmetric pattern also extremizes the Landau potential, as noted in Ref. [20], our microscopic lattice calculations find that a reflection symmetry-breaking pattern is the one selected. While, the DSL to VBC transition is allowed to be continuous, our microscopic calculations find it to be first order as inferred from a level crossing of the energies of the two states [see Fig. 2(a)] together with the observation of an abrupt change in the nearest-neighbor spin-spin correlation profile. We show that the energy gain of the VBC with respect to the $U(1)$ DSL is nonzero for $J/J_1 > 0.26(1)$ and remains so on all finite-size systems we simulated, indicating size consistency of the VBC state and its stability in the thermodynamic limit.

Further support for the pinwheel VBC state comes from mVMC calculations at $J/J_1 = 0.4$, for which we measure the

real space dimer-dimer correlation pattern (see Fig. S6 in Supplemental Material [59]) where the development of the $C_6$ symmetric pinwheel VBC is also manifest. We also construct a symmetry-breaking dimer operator with nonvanishing susceptibility extrapolated to the thermodynamic limit (see Fig. S7 in Supplemental Material [59]). An analysis of the latter suggests a triply degenerate $C_3$-related order parameter, with the three momenta $M$ points setting the spatial dependence, which signals a VBC behavior with the spontaneous $C_3$-symmetry breaking. However, the equal-weight sum of these three basis functions of the dominant irreducible representations results in an effective $C_6$ symmetric pinwheel pattern as obtained within VMC [see Fig. 1(b)], which we illustrate in the inset of Fig. S7 in Supplemental Material [59]. The corresponding susceptibility decreases rapidly as $J/J_1 \to 0$, substantiating a transition to a quantum spin liquid phase from the VBC.

To probe the aforementioned VBC order within DMRG, we start by imposing the pinwheel VBC pattern (via small pinning conjugate fields) in a trial wave function that is then used as initial state [see Fig. S14(a) in Supplemental Material [59]] for subsequent DMRG calculations performed with the original unperturbed Hamiltonian deep within the three $J/J_1$ regions of interest where DSL, VBC, and magnetic order were identified above, namely, at $J/J_1 = 0.2$, 0.4, and 0.65. This procedure allows us to probe the stability of the initially seeded pinwheel VBC state against these three phases or, alternatively, observe its melting into different quantum states. We see that for $J/J_1 = 0.4$ [see Fig. S14(c) in Supplemental Material [59]], the removal of the bias hardly affects the initial state, thus providing strong support for the pinwheel VBC as true ground state in this regime. This is further corroborated by the fact that at $J/J_1 = 0.2$ and 0.65, the VBC pattern is progressively washed out [see Fig. S14(b) and Fig. S14(d) in Supplemental Material [59]]. Together, these results provide further compelling evidence for the pinwheel VBC state in the range $J \in (g_1, g_2)$ [see Fig. 1(c)].

In Fourier space, the hallmark of the onset of the VBC order, as obtained within pf-FRG, is the splitting of the pinch points ($M$ points of the extended Brillouin zone), where the maxima of $\chi(\mathbf{k})$ are located for the projected DSL (see Fig. S8 of Supplemental Material [59]), into two symmetric half moons. This results in the intensity maxima now located at generic $(0, k_y)$ (and symmetry related) incommensurate points, as captured in an earlier pf-FRG study of the same model [81]. Given that, the DSL and VBC phases can also be distinguished by comparing $\chi(\mathbf{k})$ along two cuts in momentum space, i.e., $\Gamma$-$K$ and $\Gamma$-$M$ segments. More precisely, we define a "spectral measure" $\Delta\chi_k$ as the difference between the maxima along these two cuts, i.e., $\Delta\chi_k = \chi^{\max}(\mathbf{k} \in \Gamma\text{-}K) - \chi^{\max}(\mathbf{k} \in \Gamma\text{-}M)$. The splitting of the pinch point into half moons corresponds to a downturn in the value of $\Delta\chi$ (occurring at $J/J_1 = 0.28$) while the zero crossing of $\Delta\chi$ (occurring at $J/J_1 = 0.32$) indicates that the half moons become the dominant feature in $\chi(\mathbf{k})$. Based on these two signatures, we estimate the onset of VBC from pf-FRG at $J/J_1 = 0.30(2)$ [see Fig. 2(b) and Fig. S1 in Supplemental Material [59]], in good agreement with the other computational methods used. The evolution of the radius of the half moon as a function of $J/J_1$ obtained from pf-FRG is shown in Fig. 3 where, for

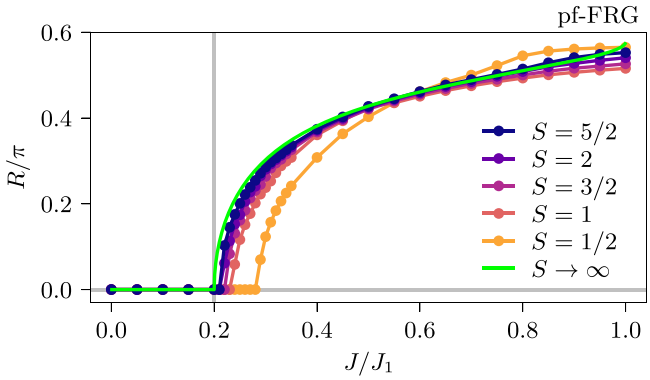


FIG. 3. Half-moon radii. From pf-FRG, we show for different values of spin $S$ [43] the evolution with $J/J_1$ of the radius of the half moons characterizing the pinwheel VBC. The large-$S$ (classical) result is from Ref. [6].

the present $S = 1/2$ model (1), one observes an appreciable deviation from the reported large-$S$ result [6]. For increasing values of $S$, the known large-$S$ behavior [6] is progressively recovered. Within the VMC calculation, the splitting of the pinch point maxima into half moons is observed deep inside the VBC phase, as shown in Fig. S9 of Supplemental Material [59]. Similarly, deep inside the VBC phase, the $\chi(\mathbf{k})$ obtained from mVMC shows maxima at incommensurate $(0, k_y)$ points, as shown in Fig. S5 of Supplemental Material [59].

Finally, we turn to the transition into the star phase. To this end, we show in Fig. 4 the evolution of the square of the sublattice magnetization $m^2$ with $J/J_1$, as obtained from mVMC, VMC, and DMRG. This quantity can be computed

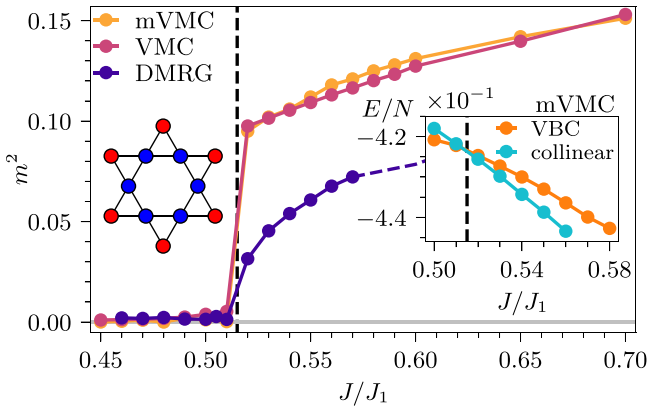


FIG. 4. Transition into the star phase. The behavior of the square of the sublattice magnetization $m^2$ with $J/J_1$ near the transition from the pinwheel VBC into collinear magnetic order (illustrated in the inset, with blue and red spins pointing in opposite directions). The results from VMC and mVMC are for a $3 \times 8 \times 8$ site cluster (see Fig. S11 in Supplemental Material [59] for finite-size scaling results of $m^2$ from VMC to the thermodynamic limit), while those from DMRG are obtained on a YC8-8 cylinder (see Supplemental Material [59] for further details). In all the three cases, $m^2$ is estimated by computing the isotropic equal-time spin-spin correlation between lattice sites separated by eight nearest-neighbor distances.

by evaluating the equal-time spin-spin correlations at the maximum distance on the finite-size lattice considered in the numerical calculation. One observes a sudden jump to a finite value of $m^2$ for $J/J_1 > 0.51(1)$, indicating the onset of long-range collinear spin order with a 12-site magnetic unit cell (see inset of Fig. 4) [52]. While the estimate of the phase boundary from these three approaches shows excellent agreement, the comparatively smaller values of $m^2$ inside the ordered phase obtained in DMRG can be ascribed to the quasi-one-dimensional character of the cylindrical geometries. The abrupt nature of the jump in the value of $m^2$ observed in mVMC and VMC, together with the crossing of the energies of the disordered VBC and magnetically ordered states across the transition point (see inset of Fig. 4), lends evidence in favor of a first-order character of the transition. Similar conclusions are drawn from VMC via finite-size scaling of $m^2$ for different values of $J/J_1$ (see Fig. S11 in Supplemental Material [59]), wherein one observes a jump in the value of $m^2$ in the thermodynamic limit. The collinear magnetically ordered state displays a starlike pattern of intensity distribution in $\chi(\mathbf{k})$ [see Fig. 1(b)] with maxima at the location expected for the octahedral regular magnetic order [53]. It is worth noting that for $S = 1/2$ the phase boundary between the half-moon and star phases considerably shifts to a smaller value of $g_2 = 0.51(1)$, compared to the classical boundary at $J/J_1 = 1$ [6], reflecting the fact that quantum fluctuations shift the helix pitch vector towards commensurate values [48,82,83].

## II. DISCUSSION

Characterizing the evolution of the ground state of the kagome antiferromagnet along the maximally frustrated $J_2 = J_{3a}$ line is a challenging endeavor. As such, it is rather satisfying to uncover a remarkable agreement between our complementary numerical approaches, these yielding a consistent understanding of the momentum and real space signatures of the ground-state phases and their respective boundaries, a feat that would not have been imaginable only a few years ago. One would expect the $U(1)$ DSL, half-moon, and star phases will display a window of stability away from the maximally frustrated $J_2 = J_{3a}$ axis. It would thus be of interest to search and identify materials promising to realize the Dirac spin liquid phase and which lie within this region of stability. The recently studied material $YCu_3(OH)_6Br_2[Br_x(OH)_{1-x}]$ [84], wherein signatures of DSL behavior have been suggested, could serve as a potential material candidate warranting further investigation. Another interesting candidate material might be the distorted kagome compound $Rb_2Cu_3SnF_{12}$ where indications for a pinwheel VBC have been reported [85]. In similar spirit, it might prove interesting to explore the corresponding quantum phase diagram on the pyrochlore lattice, which similarly at the classical level is host to persistent flat bands, as well as half-moon and star phases [6,16]. Finally, the quantum-classical correspondence in the obtained structure factors hints at a deeper connection which would constitute an exciting direction of future study.

## ACKNOWLEDGMENTS

We thank Federico Becca, Subhro Bhattacharjee, Ludovic Jaubert, Harald Jeschke, Arnaud Ralko, and Arnab Sen for insightful discussions. D.K., N.N., J.R., and S.T. acknowledge support from the Deutsche Forschungsgemeinschaft (DFG), Grant No. 277101999 CRC 183 (Project No. A04). F.F. acknowledges support from the Alexander von Humboldt Foundation through a postdoctoral Humboldt fellowship, from DFG Grant No. TRR 288 - 422213477 (project A05), and IIT Madras for funding a one-month stay through an International Visiting Postdoc travel award which facilitated the completion of this research work. N.A. is funded by the Swiss National Science Foundation, Grant No. PP00P2_176877. The mVMC simulations were supported by RSF Grant No. 21-12-00237. The work in Würzburg was supported by DFG Grant No. 258499086-SFB 1170 and the Würzburg-Dresden Cluster of Excellence on Complexity and Topology in Quantum Matter, Grant No. 390858490-EXC 2147. M.J.P.G. acknowledges support from the Canada Research Chair Program (Tier I). Y.I. acknowledges support from the Department of Science and Technology, India, Grant No. SRG/2019/000056; MATRICS Grant No. MTR/2019/001042; the Indo-French Centre for the Promotion of Advanced Research, Grant No. 64T3-1; the ICTP through the Associates Programme; and the Simons Foundation, Grant No. 284558FY19. This research was supported in part by the National Science Foundation under Grant No. NSF PHY-1748958; IIT Madras through the Institute of Eminence (IoE) program for establishing the QuCenDiEM group (Grant No. SP22231244CPMOEXQCDHOC); and the International Centre for Theoretical Sciences, Bengaluru, India during a visit for participating in the program "Frustrated Metals and Insulators" (Grant No. ICTS/frumi2022/9). N.N. thanks IIT Madras for funding a three-month stay through an International Graduate Student Travel award which facilitated completion of this research work. J.R. thanks IIT Madras for a Visiting Faculty Fellow position under the IoE program during which part of the research work and Letter writing were carried out. D.K. and S.T. acknowledge usage of the JURECA Booster and JUWELS cluster at the Forschungszentrum Juelich and the Noctua2 cluster at the Paderborn Center for Parallel Computing ($PC^2$). N.N. and J.R. acknowledge the use of the CURTA cluster at FU Berlin [86] and the JUWELS cluster at the Forschungszentrum Jülich. N.A. acknowledges the usage of computing resources of the federal collective usage center "Complex for simulation and data processing for mega-science facilities" at NRC "Kurchatov Institute". T.M., P.G., and R.T. gratefully acknowledge the Gauss Centre for Supercomputing e.V. for funding this project by providing computing time on the GCS Supercomputer SuperMUC at Leibniz Supercomputing Centre. Y.I. acknowledges the use of the computing resources at HPCE, IIT Madras.

[1] J. T. Chalker, P. C. W. Holdsworth, and E. F. Shender, Hidden Order in a Frustrated System: Properties of the Heisenberg Kagomé Antiferromagnet, Phys. Rev. Lett. **68**, 855 (1992).

[2] I. Ritchey, P. Chandra, and P. Coleman, Spin folding in the two-dimensional Heisenberg kagomé antiferromagnet, Phys. Rev. B **47**, 15342 (1993).

[3] C. L. Henley, The "Coulomb Phase" in Frustrated Systems, Annu. Rev. Condens. Matter Phys. **1**, 179 (2010).

[4] D. A. Garanin and B. Canals, Classical spin liquid: Exact solution for the infinite-component antiferromagnetic model on the kagomé lattice, Phys. Rev. B **59**, 443 (1999).

[5] M. E. Zhitomirsky, Octupolar ordering of classical kagome antiferromagnets in two and three dimensions, Phys. Rev. B **78**, 094423 (2008).

[6] T. Mizoguchi, L. D. C. Jaubert, R. Moessner, and M. Udagawa, Magnetic clustering, half-moons, and shadow pinch points as signals of a proximate Coulomb phase in frustrated Heisenberg magnets, Phys. Rev. B **98**, 144446 (2018).

[7] T. Li, A continuous family of fully frustrated Heisenberg models on the Kagome lattice, Europhys. Lett. **133**, 47001 (2021).

[8] J. M. Luttinger, A Note on the Ground State in Antiferromagnetics, Phys. Rev. **81**, 1015 (1951).

[9] J. M. Luttinger and L. Tisza, Theory of Dipole Interaction in Crystals, Phys. Rev. **70**, 954 (1946).

[10] D. H. Lyons and T. A. Kaplan, Method for Determining Ground-State Spin Configurations, Phys. Rev. **120**, 1580 (1960).

[11] J. Robert, B. Canals, V. Simonet, and R. Ballou, Propagation and Ghosts in the Classical Kagome Antiferromagnet, Phys. Rev. Lett. **101**, 117207 (2008).

[12] A. L. Chernyshev and M. E. Zhitomirsky, Order and excitations in large-$S$ kagome-lattice antiferromagnets, Phys. Rev. B **92**, 144415 (2015).

[13] Half-moons also appear for Ising models on the kagome and pyrochlore lattices for $0 < J/J_1 < 1/3$ [15] and $0 < J/J_1 < 1/4$ [16,17], respectively.

[14] H. Yan, R. Pohle, and N. Shannon, Half moons are pinch points with dispersion, Phys. Rev. B **98**, 140402(R) (2018).

[15] T. Mizoguchi, L. D. C. Jaubert, and M. Udagawa, Clustering of Topological Charges in a Kagome Classical Spin Liquid, Phys. Rev. Lett. **119**, 077207 (2017).

[16] J. G. Rau and M. J. P. Gingras, Spin slush in an extended spin ice model, Nat. Commun. **7**, 12234 (2016).

[17] M. Udagawa, L. D. C. Jaubert, C. Castelnovo, and R. Moessner, Out-of-equilibrium dynamics and extended textures of topological defects in spin ice, Phys. Rev. B **94**, 104416 (2016).

[18] M. B. Hastings, Dirac structure, RVB, and Goldstone modes in the kagomé antiferromagnet, Phys. Rev. B **63**, 014413 (2000).

[19] M. Hermele, Y. Ran, P. A. Lee, and X.-G. Wen, Properties of an algebraic spin liquid on the kagome lattice, Phys. Rev. B **77**, 224413 (2008).

[20] X.-Y. Song, C. Wang, A. Vishwanath, and Y.-C. He, Unifying description of competing orders in two-dimensional quantum magnets, Nat. Commun. **10**, 4254 (2019).

[21] Y. Iqbal, F. Becca, S. Sorella, and D. Poilblanc, Gapless spin-liquid phase in the kagome spin-$\frac{1}{2}$ Heisenberg antiferromagnet, Phys. Rev. B **87**, 060405(R) (2013).

[22] Y. Iqbal, D. Poilblanc, and F. Becca, Vanishing spin gap in a competing spin-liquid phase in the kagome Heisenberg antiferromagnet, Phys. Rev. B **89**, 020407(R) (2014).

[23] Y. Iqbal, F. Becca, and D. Poilblanc, Projected wave function study of $\mathbb{Z}_2$ spin liquids on the kagome lattice for the spin-$\frac{1}{2}$ quantum Heisenberg antiferromagnet, Phys. Rev. B **84**, 020407(R) (2011).

[24] Y.-C. He, M. P. Zaletel, M. Oshikawa, and F. Pollmann, Signatures of Dirac Cones in a DMRG Study of the Kagome Heisenberg Model, Phys. Rev. X **7**, 031020 (2017).

[25] Y. Iqbal, F. Ferrari, A. Chauhan, A. Parola, D. Poilblanc, and F. Becca, Gutzwiller projected states for the $J_1 - J_2$ Heisenberg model on the Kagome lattice: Achievements and pitfalls, Phys. Rev. B **104**, 144406 (2021).

[26] Y. Iqbal, D. Poilblanc, and F. Becca, Spin-$\frac{1}{2}$ Heisenberg $J_1$–$J_2$ antiferromagnet on the kagome lattice, Phys. Rev. B **91**, 020402(R) (2015).

[27] L. Messio, B. Bernu, and C. Lhuillier, Kagome Antiferromagnet: A Chiral Topological Spin Liquid? Phys. Rev. Lett. **108**, 207204 (2012).

[28] C.-Y. Lee, B. Normand, and Y.-J. Kao, Gapless spin liquid in the kagome Heisenberg antiferromagnet with Dzyaloshinskii-Moriya interactions, Phys. Rev. B **98**, 224414 (2018).

[29] F. Becca and S. Sorella, *Quantum Monte Carlo Approaches for Correlated Systems* (Cambridge University, Cambridge, England, 2017).

[30] T. Misawa, S. Morita, K. Yoshimi, M. Kawamura, Y. Motoyama, K. Ido, T. Ohgoe, M. Imada, and T. Kato, mVMCOpen-source software for many-variable variational Monte Carlo method, Comput. Phys. Commun. **235**, 447 (2019).

[31] D. Tahara and M. Imada, Variational Monte Carlo Method Combined with Quantum-Number Projection and Multi-Variable Optimization, J. Phys. Soc. Jpn. **77**, 114701 (2008).

[32] T. Misawa and M. Imada, Origin of high-$T_c$ superconductivity in doped Hubbard models and their extensions: Roles of uniform charge fluctuations, Phys. Rev. B **90**, 115137 (2014).

[33] M. Casula, C. Attaccalite, and S. Sorella, Correlated geminal wave function for molecules: An efficient resonating valence bond approach, J. Chem. Phys. **121**, 7110 (2004).

[34] S. Morita, R. Kaneko, and M. Imada, Quantum Spin Liquid in Spin 1/2 $J_1J_2$ Heisenberg Model on Square Lattice: Many-Variable Variational Monte Carlo Study Combined with Quantum-Number Projections, J. Phys. Soc. Jpn. **84**, 024720 (2015).

[35] Y. Nomura and M. Imada, Dirac-Type Nodal Spin Liquid Revealed by Refined Quantum Many-Body Solver Using Neural-Network Wave Function, Correlation Ratio, and Level Spectroscopy, Phys. Rev. X **11**, 031034 (2021).

[36] S. Sorella, Green Function Monte Carlo with Stochastic Reconfiguration, Phys. Rev. Lett. **80**, 4558 (1998).

[37] G. Carleo and M. Troyer, Solving the quantum many-body problem with artificial neural networks, Science **355**, 602 (2017).

[38] N. Astrakhantsev, T. Westerhout, A. Tiwari, K. Choo, A. Chen, M. H. Fischer, G. Carleo, and T. Neupert, Broken-Symmetry Ground States of the Heisenberg Model on the Pyrochlore Lattice, Phys. Rev. X **11**, 041021 (2021).

[39] J. Reuther and P. Wölfle, $J_1$–$J_2$ frustrated two-dimensional Heisenberg model: Random phase approximation and functional renormalization group, Phys. Rev. B **81**, 144410 (2010).

[40] J. Thoenniss, M. K. Ritter, F. B. Kugler, J. von Delft, and M. Punk, Multiloop Pseudofermion Functional Renormalization

for Quantum Spin Systems: Application to the Spin-$\frac{1}{2}$ Kagome Heisenberg Model, arXiv:2011.01268 v1.

[41] D. Kiese, F. L. Buessen, C. Hickey, S. Trebst, and M. M. Scherer, Emergence and stability of spin-valley entangled quantum liquids in moiré heterostructures, Phys. Rev. Res. **2**, 013370 (2020).

[42] F. L. Buessen, M. Hering, J. Reuther, and S. Trebst, Quantum Spin Liquids in Frustrated Spin-1 Diamond Antiferromagnets, Phys. Rev. Lett. **120**, 057201 (2018).

[43] M. L. Baez and J. Reuther, Numerical treatment of spin systems with unrestricted spin length $S$: A functional renormalization group study, Phys. Rev. B **96**, 045144 (2017).

[44] D. Kiese, T. Müller, Y. Iqbal, R. Thomale, and S. Trebst, Multiloop functional renormalization group approach to quantum spin systems, Phys. Rev. Res. **4**, 023185 (2022).

[45] PFFRGSolver.jl repository, https://github.com/dominikkiese/PFFRGSolver.jl.

[46] A. Keleş and E. Zhao, Rise and fall of plaquette order in the Shastry-Sutherland magnet revealed by pseudofermion functional renormalization group, Phys. Rev. B **105**, L041115 (2022).

[47] M. Hering, V. Noculak, F. Ferrari, Y. Iqbal, and J. Reuther, Dimerization tendencies of the pyrochlore Heisenberg antiferromagnet: A functional renormalization group perspective, Phys. Rev. B **105**, 054426 (2022).

[48] Y. Iqbal, P. Ghosh, R. Narayanan, B. Kumar, J. Reuther, and R. Thomale, Intertwined nematic orders in a frustrated ferromagnet, Phys. Rev. B **94**, 224403 (2016).

[49] S. R. White, Density Matrix Formulation for Quantum Renormalization Groups, Phys. Rev. Lett. **69**, 2863 (1992).

[50] M. Fishman, S. R. White, and E. M. Stoudenmire, The ITensor Software Library for Tensor Network Calculations arXiv:2007.14822.

[51] We note that a gapped $\mathbb{Z}_2$ quantum spin liquid also displays soft maxima at the pinch points as reported in Ref. [68] for the so-called $\mathbb{Z}_2[0,\pi]\beta$ state of Ref. [72]. While the $\mathbb{Z}_2[0,\pi]\beta$ state is optimal on small finite clusters, an accurate finite-size scaling shows that it reduces to the $U(1)$ DSL in the thermodynamic limit as shown in Ref. [62]. The presence of pinch points and bowtie features also in the quantum model raises interesting questions on how the gauge-field fluctuations introduced through the Gutzwiller constraint in VMC could possibly be related to an emergent electrodynamic field in the classical model.

[52] V. Grison, P. Viot, B. Bernu, and L. Messio, Emergent Potts order in the kagome $J_1 - J_3$ Heisenberg model, Phys. Rev. B **102**, 214424 (2020).

[53] L. Messio, C. Lhuillier, and G. Misguich, Lattice symmetries and regular magnetic orders in classical frustrated antiferromagnets, Phys. Rev. B **83**, 184401 (2011).

[54] T. Wang, X. Cai, K. Chen, N. V. Prokof'ev, and B. V. Svistunov, Quantum-to-classical correspondence in two-dimensional Heisenberg models, Phys. Rev. B **101**, 035132 (2020).

[55] A. V. Chubukov, S. Sachdev, and T. Senthil, Quantum phase transitions in frustrated quantum antiferromagnets, Nucl. Phys. B **426**, 601 (1994).

[56] S. Chakravarty, B. I. Halperin, and D. R. Nelson, Two-dimensional quantum Heisenberg antiferromagnet at low temperatures, Phys. Rev. B **39**, 2344 (1989).

[57] S. Chakravarty, B. I. Halperin, and D. R. Nelson, Low-Temperature Behavior of Two-Dimensional Quantum Antiferromagnets, Phys. Rev. Lett. **60**, 1057 (1988).

[58] T. Lugan, L. D. C. Jaubert, M. Udagawa, and A. Ralko, Schwinger boson theory of the $J_1, J_2 = J_3$ kagome antiferromagnet, Phys. Rev. B **106**, L140404 (2022).

[59] See Supplemental Material at http://link.aps.org/supplemental/10.1103/PhysRevResearch.5.L012025 for the methodological details for VMC, mVMC, PFFRG, and DMRG approaches together with further results and analysis.

[60] Y. Iqbal, W.-J. Hu, R. Thomale, D. Poilblanc, and F. Becca, Spin liquid nature in the Heisenberg $J_1 - J_2$ triangular antiferromagnet, Phys. Rev. B **93**, 144411 (2016).

[61] N. Astrakhantsev, F. Ferrari, N. Niggemann, T. Müller, A. Chauhan, A. Kshetrimayum, P. Ghosh, N. Regnault, R. Thomale, J. Reuther, T. Neupert, and Y. Iqbal, Pinwheel valence bond crystal ground state of the spin-$\frac{1}{2}$ Heisenberg antiferromagnet on the shuriken lattice, Phys. Rev. B **104**, L220408 (2021).

[62] Y. Iqbal, D. Poilblanc, R. Thomale, and F. Becca, Persistence of the gapless spin liquid in the breathing kagome Heisenberg antiferromagnet, Phys. Rev. B **97**, 115127 (2018).

[63] Y. Ran, M. Hermele, P. A. Lee, and X.-G. Wen, Projected-Wave-Function Study of the Spin-1/2 Heisenberg Model on the Kagomé Lattice, Phys. Rev. Lett. **98**, 117205 (2007).

[64] H. J. Liao, Z. Y. Xie, J. Chen, Z. Y. Liu, H. D. Xie, R. Z. Huang, B. Normand, and T. Xiang, Gapless Spin-Liquid Ground State in the $S = 1/2$ Kagome Antiferromagnet, Phys. Rev. Lett. **118**, 137202 (2017).

[65] S. S. Jahromi, R. Orús, D. Poilblanc, and F. Mila, Spin-$\frac{1}{2}$ kagome Heisenberg antiferromagnet with strong breathing anisotropy, SciPost Phys. **9**, 092 (2020).

[66] W. Zhu, X. Chen, Y.-C. He, and W. Witczak-Krempa, Entanglement signatures of emergent Dirac fermions: Kagome spin liquid and quantum criticality, Sci. Adv. **4**, eaat5535 (2018).

[67] R.-Y. Sun, H.-K. Jin, H.-H. Tu, and Y. Zhou, Possible chiral spin liquid state in the $S = 1/2$ kagome Heisenberg model, arXiv:2203.07321 (2022).

[68] C. Zhang and T. Li, Variational study of the ground state and spin dynamics of the spin-$\frac{1}{2}$ kagome antiferromagnetic Heisenberg model and its implication for herbertsmithite $ZnCu_3(OH)_6Cl_2$, Phys. Rev. B **102**, 195106 (2020).

[69] J.-W. Mei, J.-Y. Chen, H. He, and X.-G. Wen, Gapped spin liquid with $\mathbb{Z}_2$ topological order for the kagome Heisenberg model, Phys. Rev. B **95**, 235107 (2017).

[70] S. Yan, D. A. Huse, and S. R. White, Spin-Liquid Ground State of the $S = 1/2$ Kagome Heisenberg Antiferromagnet, Science **332**, 1173 (2011).

[71] M. Hering, J. Sonnenschein, Y. Iqbal, and J. Reuther, Characterization of quantum spin liquids and their spinon band structures via functional renormalization, Phys. Rev. B **99**, 100405(R) (2019).

[72] Y.-M. Lu, Y. Ran, and P. A. Lee, $\mathbb{Z}_2$ spin liquids in the $S = \frac{1}{2}$ Heisenberg model on the kagome lattice: A projective symmetry-group study of Schwinger fermion mean-field states, Phys. Rev. B **83**, 224413 (2011).

[73] S. Bieri, L. Messio, B. Bernu, and C. Lhuillier, Gapless chiral spin liquid in a kagome Heisenberg model, Phys. Rev. B **92**, 060407(R) (2015).

[74] S. Bieri, C. Lhuillier, and L. Messio, Projective symmetry group classification of chiral spin liquids, Phys. Rev. B **93**, 094437 (2016).

[75] R. Schaffer, Y. Huh, K. Hwang, and Y. B. Kim, Quantum spin liquid in a breathing kagome lattice, Phys. Rev. B **95**, 054410 (2017).

[76] Y. Iqbal, F. Becca, and D. Poilblanc, Valence-bond crystals in the kagomé spin-1/2 Heisenberg antiferromagnet: a symmetry classification and projected wave function study, New J. Phys. **14**, 115031 (2012).

[77] Y. Iqbal, F. Becca, and D. Poilblanc, Valence-bond crystal in the extended kagome spin-$\frac{1}{2}$ quantum Heisenberg antiferromagnet: A variational Monte Carlo approach, Phys. Rev. B **83**, 100404(R) (2011).

[78] R. R. P. Singh and D. A. Huse, Ground state of the spin-1/2 kagome-lattice Heisenberg antiferromagnet, Phys. Rev. B **76**, 180407(R) (2007).

[79] Y. Huh, M. Punk, and S. Sachdev, Vison states and confinement transitions of $\mathbb{Z}_2$ spin liquids on the kagome lattice, Phys. Rev. B **84**, 094419 (2011).

[80] More specifically, this particular expectation value of the monopole extremizes the invariant given in Eq. (8) of Ref. [20] that is constructed out of the monopole and mass terms.

[81] F. L. Buessen and S. Trebst, Competing magnetic orders and spin liquids in two- and three-dimensional kagome systems: Pseudofermion functional renormalization group perspective, Phys. Rev. B **94**, 235138 (2016).

[82] A. V. Chubukov, On the quantum effects in helimagnets, J. Phys. C **17**, L991 (1984).

[83] P. Ghosh, T. Müller, F. P. Toldin, J. Richter, R. Narayanan, R. Thomale, J. Reuther, and Y. Iqbal, Quantum paramagnetism and helimagnetic orders in the Heisenberg model on the body centered cubic lattice, Phys. Rev. B **100**, 014420 (2019).

[84] Z. Zeng, X. Ma, S. Wu, H.-F. Li, Z. Tao, X. Lu, X.-h. Chen, J.-X. Mi, S.-J. Song, G.-H. Cao, G. Che, K. Li, G. Li, H. Luo, Z. Y. Meng, and S. Li, Possible Dirac quantum spin liquid in the kagome quantum antiferromagnet $YCu_3(OH)_6Br_2[Br_x(OH)_{1-x}]$, Phys. Rev. B **105**, L121109 (2022).

[85] K. Matan, T. Ono, Y. Fukumoto, T. J. Sato, J. Yamaura, M. Yano, K. Morita, and H. Tanaka, Pinwheel valence-bond solid and triplet excitations in the two-dimensional deformed kagome lattice, Nat. Phys. **6**, 865 (2010).

[86] L. Bennett, B. Melchers, and B. Proppe, Curta: A general-purpose high-performance computer at ZEDAT, Freie Universität Berlin (2020), doi: 10.17169/refubium-26754.